# A Tissue-Channel Transcutaneous Power Transfer Technique for Implantable Devices

Pengpeng Chen, Huazhong Yang, *Senior Member, IEEE*, Rong Luo, and Bo Zhao, *Senior Member, IEEE*

***Abstract*—For implantable devices, miniaturization is a key design consideration, which facilitates keyhole surgery and relieves the surgical pain. Wireless power transfer is a commonly used way for implants, and a high power transfer efficiency (PTE) could help to minimize or even remove the battery inside the human body. Conventionally, the required power is delivered transcutaneously to a medical implant by inductive coupling or capacitive coupling, but the PTE is extremely low when targeting at a very small implant through a thick tissue layer. In this paper, we propose a new technique by utilizing the body tissue as the power transfer channel, where a pair of medical electrodes are attached on the body surface to supply power to a miniaturized implant with a differential input. The PTE is remarkably improved by the current loop through the body tissue without violating the IEEE specific absorption rate standard. Measurement results show that the tissue-channel technique achieves 0.39% PTE for a 1-mm-sized implant locating 5 cm deep inside the tissue.**

***Index Terms*—Implantable device, miniaturization, power transfer efficiency (PTE), specific absorption rate (SAR), tissue channel, transcutaneous power transfer.**

## I. Introduction

WIRELESS power transfer (WPT) is a conventional way to deliver power to implanted devices. The use of transcutaneous wires to power an implant causes discomfort to the patient and increases the risk of infection, whereas the battery-only solution leads to a large size of implant and requires a surgical procedure for device insertion or replacement [1]. The commonly used WPT methods are based on inductive coupling or capacitive coupling [2]–[6]. The inductive coupling [2], [3], [7]–[11] drives the transmitting (Tx) coil outside the human body to power an implant with a receiving (Rx) coil, where the energy is transferred wirelessly through the mutual coupling between the two coils. The capacitive coupling WPT [5], [6] adopts two capacitors, where one plate of each capacitor is implanted into the body, and the power is transferred through the two capacitors. The inductive/capacitive coupling WPT either directly provides energy for the implant or charges the battery to extend the lifespan.

The power transfer efficiency (PTE) of the conventional WPT schemes is significantly limited by both the dimension and insertion depth of the implant. For inductive coupling, the implant should be implemented with a 2-D or 3-D Rx coil for power harvesting [12]–[15]. Targeting at a relative large implant coil of 4.5 mm $\times$ 4.5 mm [16], the inductive power link demonstrated a 4.3% PTE at an insertion depth of 1.2 cm. Coil segmentation with resonant capacitors was used to eliminate the dielectric loss to improve the PTE to 75% [4], [17], while the insertion depth of 10.7 cm was achieved by enlarging the implant coil to be 5.3 cm in diameter. As the size of implant was reduced to 1 mm, a 2-D antenna in [14] showed a reduced PTE of 0.56% at the same insertion depth as [16], while the PTE was increased to 0.93% at a depth of 3 cm by employing a 3-D antenna [15]. By load optimization, the PTE reached 1.4% for a 1-mm implant coil locating 1 cm below the skin [12]. However, the insertion depths in all the reported works [12], [14]–[16] were limited to less than 3 cm. Although the power transfer distance was extended to 5 cm for a 2 mm $\times$ 2 mm Rx antenna [13], it led to a much lower PTE of 0.025%. To obtain a sufficient PTE beyond 5 cm, the implant had to include a large coil, e.g., 25 mm $\times$ 10 mm in [2], 10 mm $\times$ 10 mm in [9] and [11], and 40-mm diameter in [10]. Even worse, capacitive coupling [5], [18], [19] is generally limited to subcutaneous devices at a millimeter-level insertion depth. For example, [5] and [18] employed capacitive coupling for 3- and 5-mm insertion depths, respectively. Moreover, the dimensions of implanted capacitor plates were much larger, i.e., 200 and 380 mm$^2$, in [5] and [18]. Ultrasonic power transfer can realize a higher PTE, but it needs a piezoelectric sensor, which results in much higher cost [20]–[24].

In the applications of cardiac care or endoscopy, it is necessary to deliver power to a tiny implant locating deeply inside the body. For an insertion depth of 5 cm, the state-of-the-art WPT systems achieve a maximal PTE of 0.025% for a 2 mm $\times$ 2 mm implant [13]. In this paper, we propose a new power transfer technique to improve the transcutaneous PTE. Instead of conventional inductive-coupling and capacitive-coupling WPT methods, the body tissue is utilized as the power transfer medium without violating the specific absorption rate (SAR) standard. A prototype is implemented by a 1-mm-sized implant inside a block of pork, and the experiment results show the PTE can be

Manuscript received May 16, 2017; revised September 18, 2017 and November 18, 2017; accepted December 27, 2017. Date of publication January 11, 2018; date of current version August 7, 2018.This work was supported by the National Natural Science Foundation of China under Grant 61204032 and the 1000 Young Talents Plan of China. Recommended for publication by Associate Editor S. C. Tan. *(Corresponding author: Bo Zhao.)*

B. Zhao is with the Institute of VLSI Design, College of Information Science and Electronic Engineering, Zhejiang University, Hangzhou 310027, China (e-mail: zhaobo@zju.edu.cn).

P. Chen was with the Department of Electronic Engineering, Tsinghua University, Beijing 100084, China. He is now with the Beijing Institute of Radio Measurement, 100854, China.

H. Yang and R. Luo are with the Department of Electronic Engineering, Tsinghua University, Beijing 100084, China.

Color versions of one or more of the figures in this paper are available online at http://ieeexplore.ieee.org.

Digital Object Identifier 10.1109/TPEL.2018.2791966

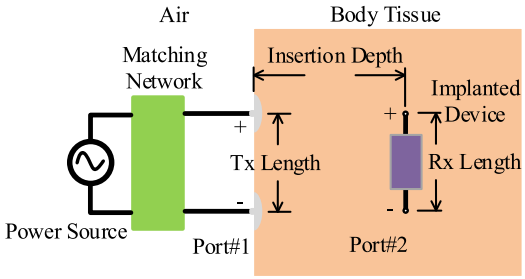


Fig. 1. Tissue-channel power transfer.

remarkably improved by the proposed technique, compared to the conventional capacitive coupling [5], [18], [19], inductive coupling [2], [9]–[11], [13], and ultrasonic [20]–[24].

The rest of this paper is organized as follows. Section II describes the theoretical analysis, and Section III displays the experiment setup. The measured results are presented and analyzed in Section IV. Finally, the conclusion remarks are drawn in Section V.

## II. Theoretical Analysis

The proposed transcutaneous power transfer technique is to use the body tissue as the power-delivery channel to reduce the transmission loss. As illustrated in Fig. 1, the implanted device at the Rx side has a differential port in contact with the internal body tissue. Outside the body, two medical electrodes are attached on the body surface, driven by a differential Tx power source. The positive Tx electrode on the body surface injects a current into the body, which goes through the body tissue and then flows into the positive electrode of the implant. Subsequently, the current goes through the implant and gets out from the negative Rx electrode and then returns to the negative Tx electrode through the body tissue. This way, a current loop is formed to deliver power from Tx electrodes to the implanted Rx device. The Tx input is matched to 50 Ω by an L-matching network, making it easy to be driven by any commercial 50-Ω power source.

The current density in the body tissue is analyzed by electromagnetic (EM) simulation. A tissue block with a dimension of 27 cm × 9 cm × 6.3 cm, a skin layer of 0.5 cm, a fat layer of 0.8 cm, and a muscle layer of 5.0 cm is modeled by the HFSS tool to study the current distribution. According to [25], we set the dielectric properties of skin fat and muscle layer in the HFSS environment. As simulated in Fig. 2, the current below the two attached Tx electrodes shows the maximal density. In addition, the current density in the fat layer is smaller than the muscle layer, and the maximal density appears in the skin layer. Therefore, the Rx device is implanted straightly below the Tx port, as illustrated in Fig. 1.

The electric field generated by Tx electrodes with different shapes is observed to study the impact to PTE. Three kinds of Tx electrodes are adopted, i.e., circular, square, and triangle, while the areas are kept to be the same to make a fair comparison. The simulation results are shown in Fig. 3, indicating that the shape of the Tx electrode has a little impact on the electric field at the location of the Rx implant.

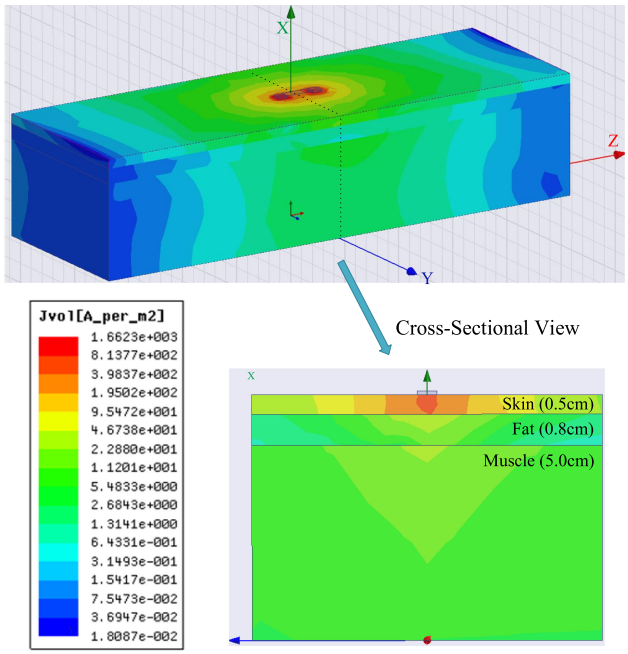


Fig. 2. Current distribution.

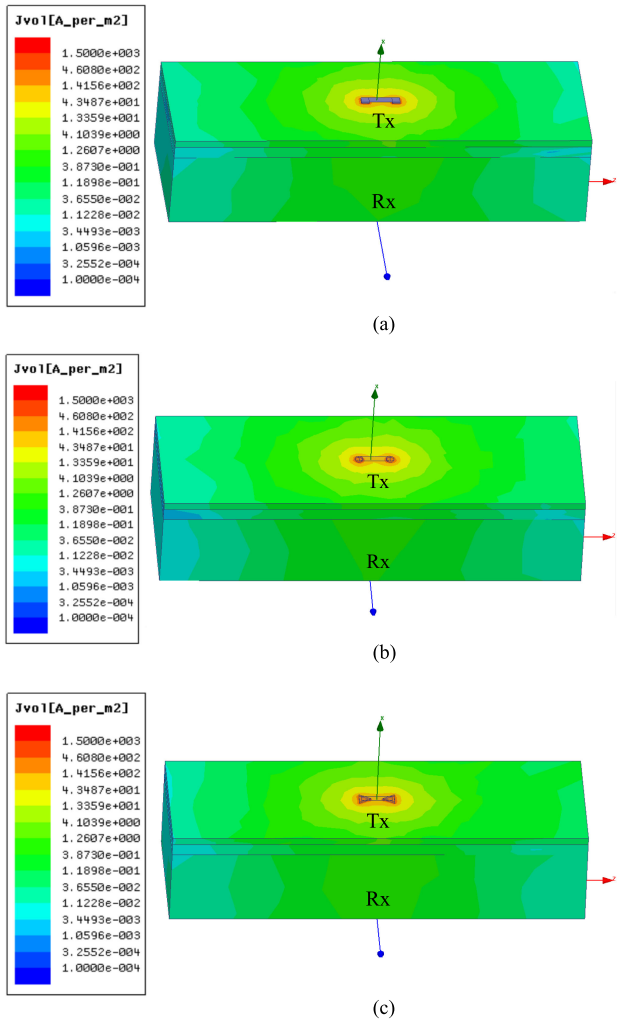


Fig. 3. Impact of electrode shapes: (a) Square, (b) round, and (c) triangle.

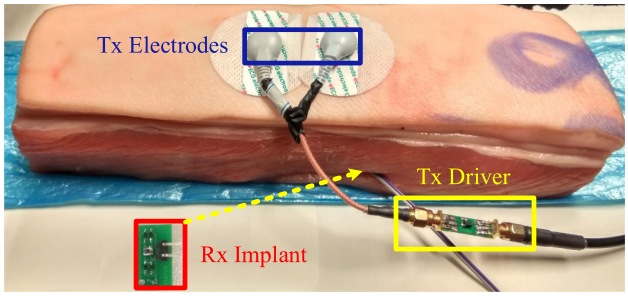


Fig. 4. Experimental setup.

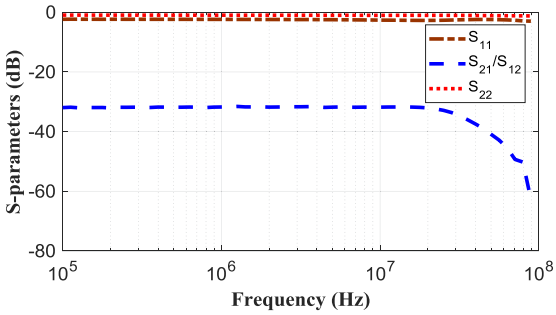


Fig. 5. Measured S-parameters.

The S-parameters of the Tx port and the Rx port are analyzed by measurement. We pick up a piece of pork belly with the same dimension and thickness as the model in the HFSS platform, and the measurement is set up in Fig. 4. The two ports of the pork tissue are corresponding to the two ports in Fig. 1, where port#1 is the Tx input on the body surface and port#2 is the Rx port implanted in the tissue. The Agilent vector network analyzer E5071C is used to measure all S-parameters of the two-port network. A group of typical S-parameters are shown in Fig. 5 with a 5-cm insertion depth, a 2-cm separation distance between the two differential Tx electrodes (named "Tx length"), and a 5-mm separation distance between the two Rx terminals (named "Rx length").

With the S-parameters of port#1 and port#2, the maximal power gain can be calculated. The power delivered to the load will reach the peak when the output impedance of port#2 matches conjugately with the load impedance. The maximal power gain $G_{\max}$ is defined as the ratio of available power at the Rx port (port#2) over the injected power at the Tx port (port#1) [26]:

$$G_{\max} = \frac{V_{\text{pp}}^2}{32\text{Re}(Z_{22})P_{\text{in}}} \tag{1}$$

where $P_{\text{in}}$ is the input power of port#1, $V_{\text{pp}}$ is the open-circuit voltage (peak to peak) of port#2, and $\text{Re}(Z_{22})$ is the real part of the port#2 impedance. The maximal power gain $G_{\max}$ versus the working frequency is plotted in Fig. 6, with an insertion depth of 5 cm, a Tx length of 2 cm, and an Rx length of 5 mm. It can be seen that $G_{\max}$ is close to $-22$ dB for the frequency below 20 MHz. This is consistent with the results in [27], which showed more power is absorbed by the body tissue at a frequency higher than 20 MHz.

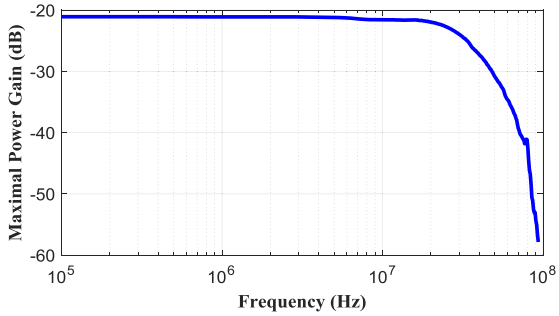


Fig. 6. Maximal power gain versus frequency.

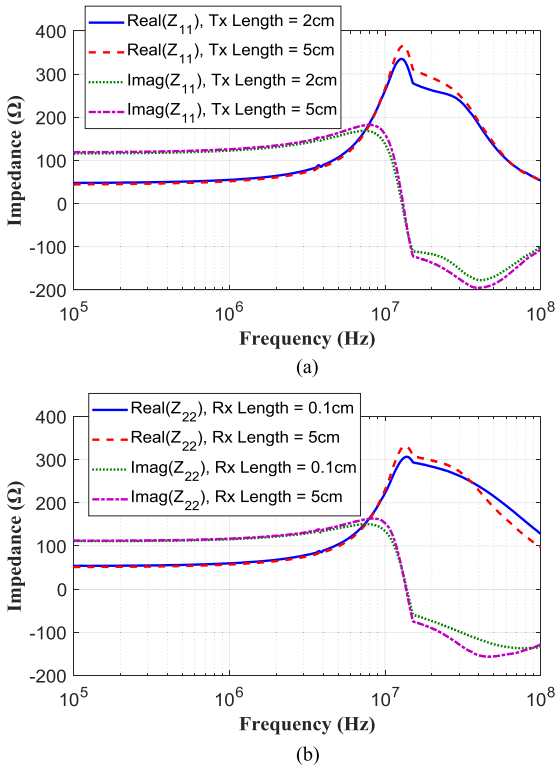


Fig. 7. (a) $Z_{11}$ versus Tx length. (b) $Z_{22}$ versus Rx length.

We investigate the influence of the Tx length and the Rx length on the input/output impedance of the power transfer system. Both the input impedance of port#1 ($Z_{11}$) and the output impedance of port#2 ($Z_{22}$) can be obtained by the measured S-parameters. As shown in Fig. 7, neither the Tx length nor the Rx length has an obvious impact on $Z_{11}$ and $Z_{22}$. This is because both $Z_{11}$ and $Z_{22}$ are mainly dominated by the contact impedance between the electrodes and the body tissue. The self-resonance frequency of port#2 stays close to 13.9 MHz when the Rx length changes from 1 to 50 mm, as shown in Fig. 8. The real part of $Z_{22}$ is about 310 Ω at the self-resonance frequency of port#2, where $Z_{11}$ is 360 + j70 Ω.

The power transfer system is reconfigured to study the changing of the maximal power gain $G_{\max}$ versus the Rx length, the Tx length, and the insertion depth. We sweep the Rx length from 0.1 to 5 cm, the TX length from 2 to 5 cm, and the insertion depth from 1 to 5 cm to observe the maximal power gain curves

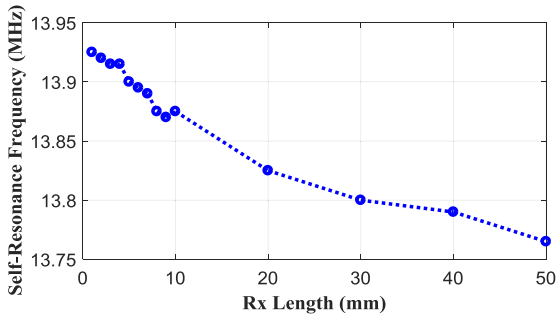


Fig. 8. Self-resonance frequency versus Rx length.

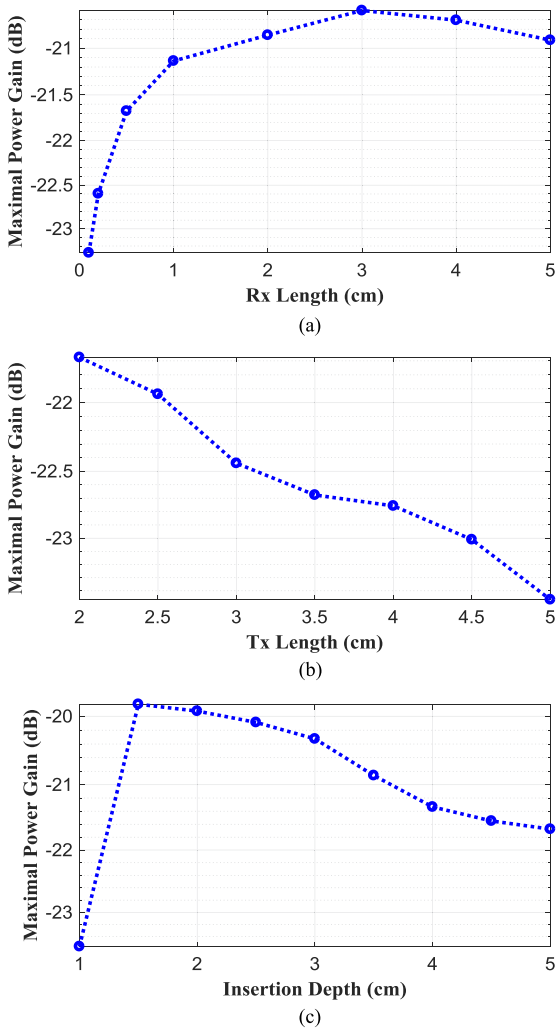


Fig. 9. (a) Power gain versus Rx length. (b) Power gain versus Tx length. (c) Power gain versus insertion depth.

in Fig. 9. At an insertion depth of 5 cm and a Tx length of 2 cm, $G_{\max}$ initially rises with the increasing of the Rx length and then goes down at an Rx length beyond 3 cm, as shown in Fig. 9(a). Fig. 9(b) illustrates the decreasing of $G_{\max}$ versus the Tx length, with an insertion depth of 5 cm and an Rx length of 5 mm. This is because the electric field at the implant becomes weaker as the two Tx electrodes move away from each other. At a Tx length of 2 cm and an Rx length of 5 mm, $G_{\max}$ decreases

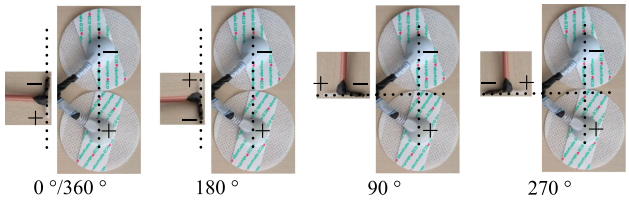


Fig. 10. Relative angles between Tx port and Rx port.

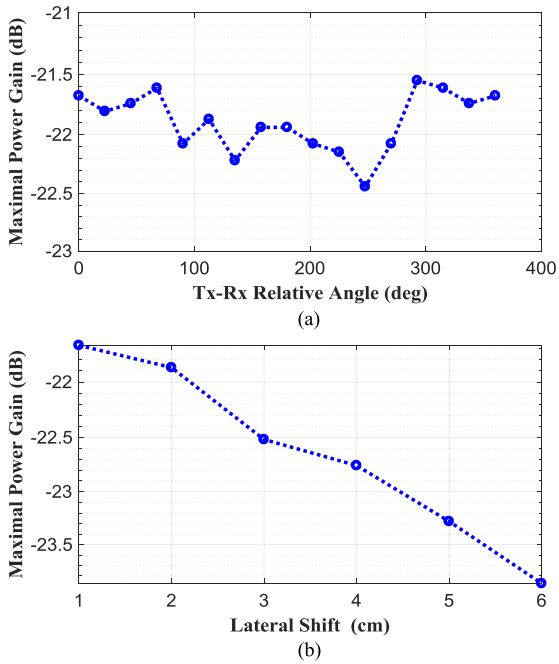


Fig. 11. (a) Maximal power gain versus Tx–Rx angle. (b) Maximal power gain versus Tx–Rx lateral shift.

as the insertion depth increases from 2 cm in Fig. 9(c). Note that the efficiency at an insertion depth of 1 cm is even smaller than the 2-cm-depth case due to the fat layer. Compared with the muscle layer, the fat layer locates at 1 cm below the skin surface, which has a much smaller electrical conductivity and a much higher contact resistance with the Rx implant.

The relative angle between the Tx port and the Rx port is analyzed in Fig. 10. With an insertion depth of 5 cm, a Tx length of 2 cm, and an Rx length of 5 mm, the maximal power gain versus the relative angle is plotted in Fig. 11(a), indicating that the relative angle has a little impact on the maximal power gain. In addition, the effect of the lateral shift is shown in Fig. 11(b), where a larger lateral shift results in a smaller power gain.

## III. Experiment Setup

An experiment is set up to validate the PTE performance of the proposed tissue-channel technique. The equivalent circuit is shown in Fig. 12, where an L-shape matching is designed to match the Tx port to 50 Ω, making it easy to be driven by a 50-Ω standard power source. At the Rx side, the rectifier is implemented by the diodes of SMS7630-079LF (SKYWORKS) with a small parasitic capacitance of 0.3 pF [28]. A 500-Ω resistor is adopted as the load of the rectifier, in parallel with

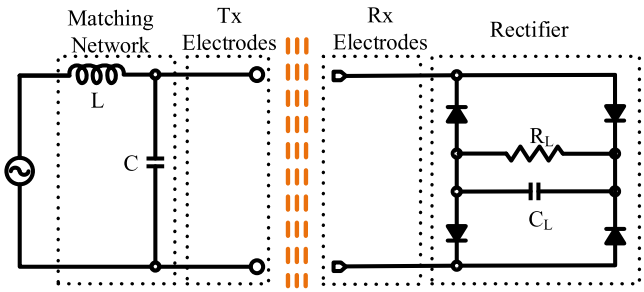


Fig. 12. Equivalent circuit of proposed power transfer system.

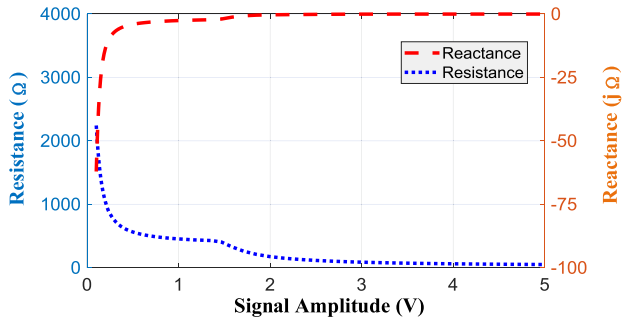


Fig. 13. Rectifier input impedance versus signal amplitude.

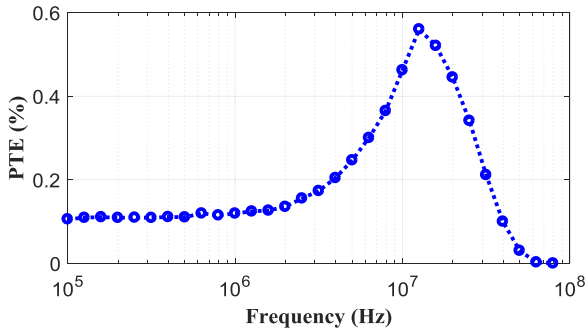


Fig. 14. Optimization of operating frequency.

a decoupling capacitor of 10 nF. The PTE is defined by the dc power achieved at the Rx load over the power generated by the power source.

The operation frequency is optimized for the maximal PTE. The input impedance of the rectifier is simulated in Fig. 13, where the reactance part turns to be very small at an input amplitude larger than 0.3 V due to the diodes. According to the equivalent circuit in Fig. 12, the output power of the signal source is set to 20 dBm, while the $L$ and $C$ in the matching network are adjusted for different frequencies to conjugately match the input impedance ($Z_{11}$) of the tissue in Fig. 7(a). The harvested dc power of the rectifier is simulated by using the Harmonic-Balance tool in Cadence. As a result, the PTE at different frequencies is obtained by the harvested dc power over the 20-dBm source power, as shown in Fig. 14. It can be seen that the PTE reaches the peak value at 13.9 MHz.

The SAR must be considered to ensure the safety of the human exposed to RF EM fields. The peak spatial average SAR value is 2 W/kg for uncontrolled environments according to IEEE Standard C95.1-2005 [29], as shown in Table I. A specific current limit is also presented in [29] for the devices in contact with human body, where the current limit is 16.7 mA time-averaged over either 6 or 30 min [29]. In our case, the input impedance of port#1 is 360 + j70 Ω at 13.9 MHz, which results in 20-dBm power with an input current of 16.7 mA. Considering the loss of the L-shape matching network, a 13.9-MHz 20-dBm sinusoidal signal can be adopted to drive the Tx port, which is safe for the body tissue.

A three-layer tissue model with a 0.5-cm skin layer, a 0.8-cm fat layer, and a 5.0-cm muscle layer is established by the CST tool to simulate the average SAR over a 10-g tissue, as shown in Fig. 15. With an input current of 16.7 mA at 13.9 MHz, the SAR is below 0.861 W/kg, which is 43% of the 2-W/kg SAR limit. If only a small part of the electrode is conducting, the contact resistance will increase. As the output power of the Tx source is fixed, the input current will decrease with the increasing of the contact resistance, which keeps the SAR below the standard limit. This way, we can make sure that the 13.9-MHz 20-dBm input Tx power will not be harmful to the human body.

## IV. Measurement Results

The proposed technique is validated by the prototype shown in Fig. 16. The rectifier is implemented on a printed circuit board (PCB), where two metal lines serve as the differential port of Rx (port#2). A 13.9-MHz sinusoidal power signal is fed to the input of the L-shape matching network by Agilent E4438C signal generator (50-Ω output resistance), and a VC9801A+ digital multimeter is used to measure the dc voltage (power) harvested at the output of the Rx rectifier.

The harvested dc voltage at the Rx side is measured for different Rx lengths, Tx lengths, and insertion depths, as shown in Fig 17. For different Rx lengths, the insertion depth and the Tx length are fixed to 5 and 2 cm, respectively. As shown in Fig 17(a), the peak value of the output voltage is achieved at an Rx length of 5 mm, which is close to 0.505 V. This is because the Tx electrodes with a 2-cm separation distance generate the maximal current density in the 5-mm zone of the Rx location. Even if the Rx length is reduced to 1 mm, we can still harvest a dc voltage of 0.44 V.

The relationship between the harvested dc voltage and the Tx length is also studied by measurement in Fig 17(b). With an Rx length of 5 mm and an insertion depth of 5 cm, a larger Tx length generates a weaker electric field in the tissue, leading to a smaller harvested dc voltage.

The harvested dc output voltage is measured for different insertion depths, as illustrated in Fig. 17(c). With an Rx length of 5 mm and a Tx length of 2 cm, the harvested dc voltage reaches the peak (0.64 V) at an insertion depth of 2 cm. These measured results are consistent with the results calculated by S-parameters in Fig. 9.

The maximal power delivery is limited by the SAR standard. According to the result in Fig. 15, the SAR is 0.861 W/kg corresponding to an output power of 0.51 mW at an Rx length of 5 mm, a Tx length of 2 cm, and an insertion depth of 5 cm as shown in Fig. 18. So, the maximum power will be 1.18 mW when the SAR reaches the standard value of 2 W/kg.

TABLE I
SAR LIMITS FOR FREQUENCIES BETWEEN 100 KHZ AND 3 GHZ [29]

| | | Action level SAR[a] (W/kg) | Persons in controlled environments SAR[a] (W/kg) |
|---|---|---|---|
| Whole-body exposure | Whole-body average | 0.08 | 0.4 |
| Localized exposure | Localized (peak spatial average) | 2 | 10 |
| Localized exposure | Extremities and pinnae | 4 | 20 |

[a]Average value over any 10-g part of the tissue (defined as a tissue volume in the shape of a cube).

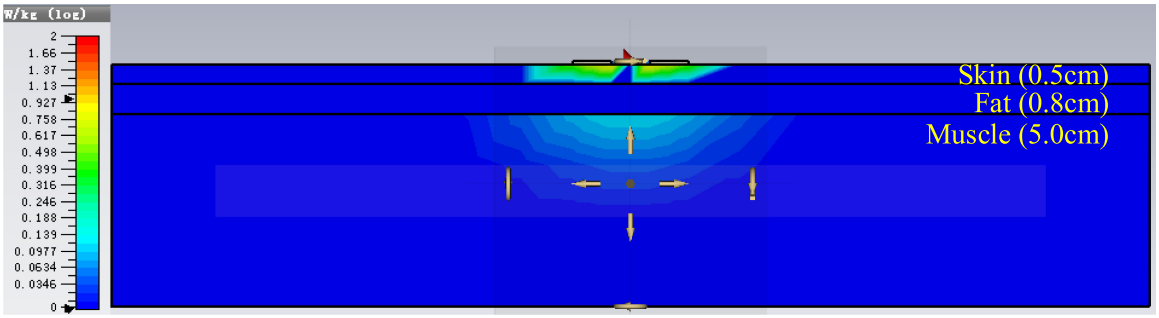


Fig. 15. SAR simulation.

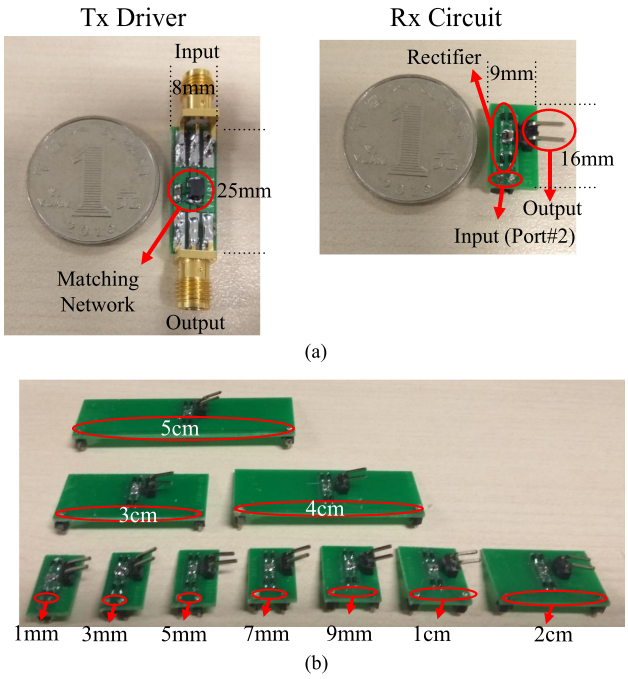


Fig. 16. (a) Tx driver and Rx circuit. (b) Rx PCBs with different Rx lengths.

The influence of the Tx electrodes' shapes is studied by measurement. We use copper electrodes in different shapes to study the impact on the PTE, as shown in Fig. 20. To make a fair comparison, all the Tx electrodes are designed to be with the same area. We set up the prototype with typical parameters, i.e., an Rx length of 5 mm, a Tx length of 2 cm, and an insertion depth of 5 cm. Measured results show that the PTE is 0.44%, 0.45%, and 0.44% for circular, square, and triangle, respectively.

The harvested dc voltage is also measured versus the different relative angles and lateral shift between the Tx port and the Rx

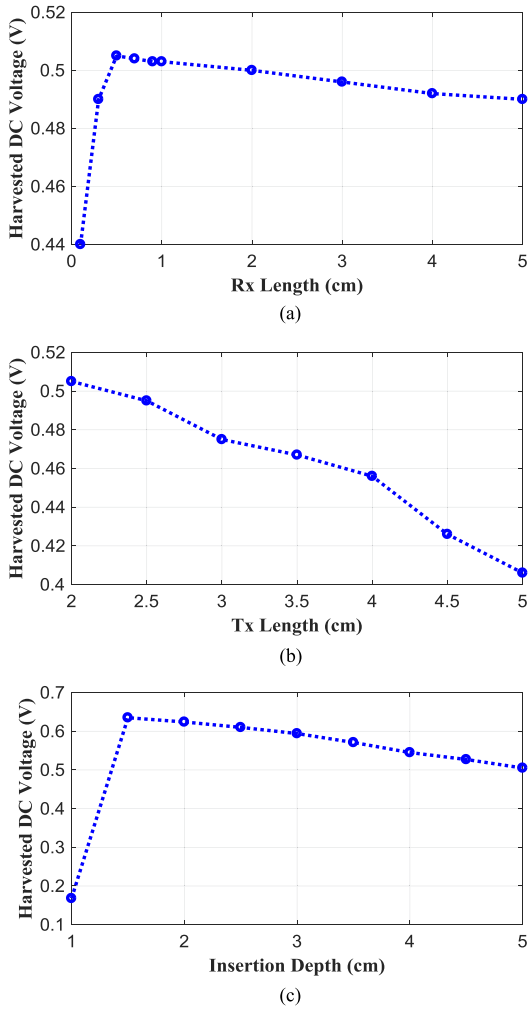


Fig. 17. (a) Harvested DC voltage versus Rx length. (b) Harvested DC voltage versus Tx length. (c) Harvested DC voltage versus insertion depth.

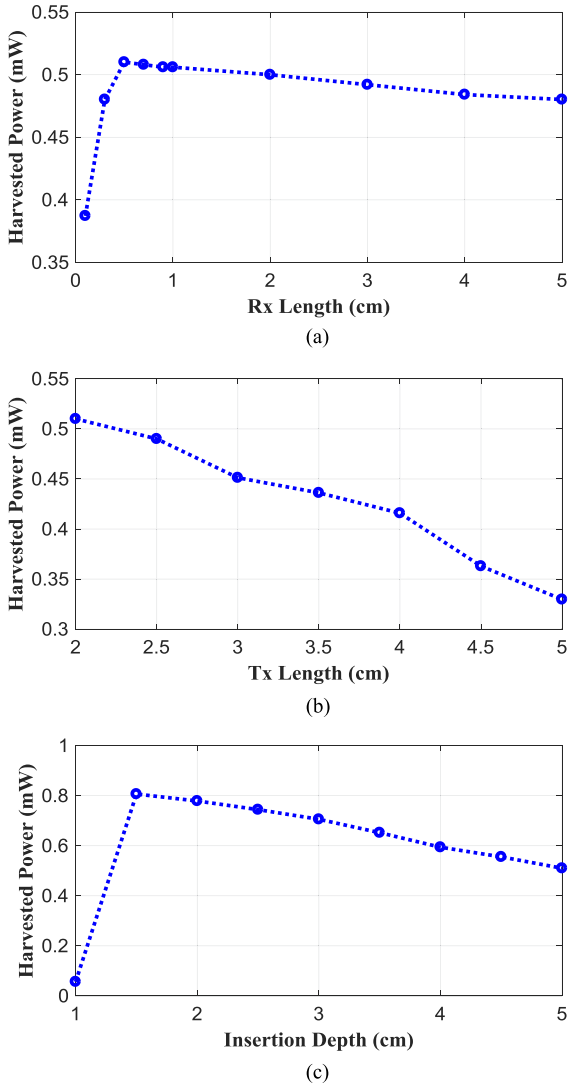


Fig. 18. (a) Harvested power versus Rx length. (b) Harvested power versus Tx length. (c) Harvested power versus insertion depth.

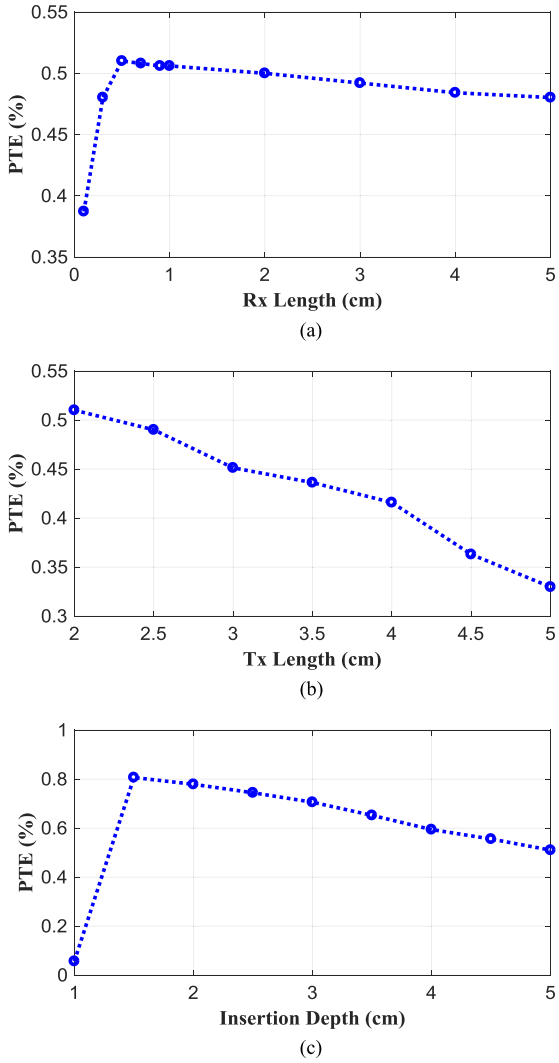


Fig. 19. (a) PTE versus Rx length. (b) PTE versus Tx length. (c) PTE versus insertion depth.

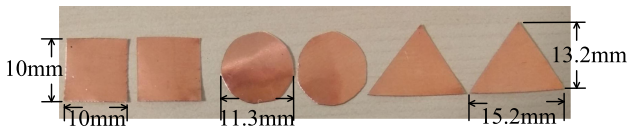


Fig. 20. Different shapes of Tx electrodes.

port, as shown in Fig. 21(a) and (b). At an insertion depth of 5 cm, a Tx length of 2 cm, and an Rx length of 5 mm, the result matches well with Fig. 11. The relative angle induces a little impact on the PTE, while a lateral shift results in a lower PTE.

The harvested dc voltage versus the apart distance between Rx electrodes and the tissue is shown in Fig. 21(c). The measurement is carried out with an Rx length of 5 mm, a Tx length of 2 cm, and an insertion depth of 5 cm. The harvested dc voltage in the noncontact case (apart distance $>0$) is much smaller than that of the in-contact case (apart distance $= 0$). As a result, the power transfer is mainly conducted by the tissue channel instead of the capacitive coupling.

Table II summarizes the performance of the proposed technique in comparison to other related works. The proposed technique shows an improved PTE with the smallest implant at an insertion depth of 5 cm. The figure of merit (FoM) in [30] only included the surface area of implant without the Tx size. In our case, the Tx electrodes are commercial ECG electrodes, whereas the Rx electrodes are two metal tips in contact with the internal tissue. The cross section of the metal tips affects the contact impedance, while the metal length does not affect the PTE. Considering that the implant size is more important than the Tx size, we set the index of the Rx size to be two times of the Tx size. So, the FoM is defined as

$$\text{FoM} = \frac{d^2 \times \text{PTE}}{\text{Rx\_Size}^{2/3} \times \text{Tx\_Size}^{1/3}}. \tag{2}$$

In our designs, the Rx implant is about 0.3 mm $\times$ 1.3 mm, where the diameter of metal tips is as small as 0.3 mm. It can be seen that the proposed technique achieves the second best FoM among the state-of-the-art works. Compared to the 5-cm-range power transfer in [2] and [13], our system achieves a $>2$ times higher PTE, although the implanted device is much smaller.

TABLE II
PERFORMANCE COMPARISON

| References | Rx size | Tx size | Insertion depth | Frequency | PTE | Method | Medium | FoM | CMOS compatible |
|---|---|---|---|---|---|---|---|---|---|
| [5], 2016 | $10 \times 20$ mm$^2$ | $40 \times 40$ mm$^2$ | 0.3 cm | 402 MHz | 35% | Capacitive | Tissue | 0.0079 | Y |
| [18], 2013 | 380 mm$^2$ | 380 mm$^2$ | 0.5 cm | 402 MHz | 67% | Capacitive | Gel | 0.044 | Y |
| [19], 2014 | 50 mm$^2$ | 50 mm$^2$ | 0.9 cm | 5 MHz | 3.13% | Capacitive | Tissue | 0.051 | Y |
| [12], 2016 | 1-mm diameter | 28-mm diameter | 1 cm | 20 MHz | 1.4% | Inductive | Tissue | 0.19 | Y |
| [14], 2016 | 1-mm diameter | 6-mm diameter | 1.2 cm | 200 MHz | 0.56% | Inductive | Tissue | 0.31 | Y |
| [16], 2013 | $4.5 \times 4.5$ mm$^2$ | $20 \times 20$ mm$^2$ | 1.2 cm | 6.5 MHz | 4.3% | Inductive | Tissue | 0.11 | Y |
| [15], 2013 | 1 mm$^3$ | N/A | 3 cm | 400 MHz | 0.93% | Inductive | Tissue | N/A | Y |
| [24], 2017 | 1.1-mm diameter | 15.9-mm diameter | 3 cm | 1.1 MHz | 0.65% | Ultrasonic | Oil | 1.04 | N |
| [31], 2015 | 1 mm $^2$ | 12.7-mm diameter | 3 cm | 1 MHz | N/A | Ultrasonic | Tissue | N/A | N |
| [32], 2015 | $0.127 \times 0.127$ mm$^2$ | 6.35-mm diameter | 3 cm | 5 MHz | 0.002% | Ultrasonic | Water | 0.09 | N |
| [13], 2012 | $2 \times 2$ mm$^2$ | $40 \times 40$ mm$^2$ | 5 cm | 1.86 GHz | 0.025% | Inductive | Water | 0.021 | Y |
| [2], 2013 | $25 \times 10$ mm$^2$ | $67 \times 27$ mm$^2$ | 5 cm | 13.56 MHz | 0.16% | Inductive | Tissue | 0.008 | Y |
| [23], 2015 | 5 mm $^2$ | 20-mm diameter | 20 cm | 2.3 MHz | 0.4% | Ultrasonic | Water | 8.05 | N |
| This work | $0.3 \times 1.3$ mm$^2$ | $8 \times 28$ mm$^2$ | 5 cm | 13.9 MHz | 0.39% | Tissue-channel | Tissue | 3.01 | Y |

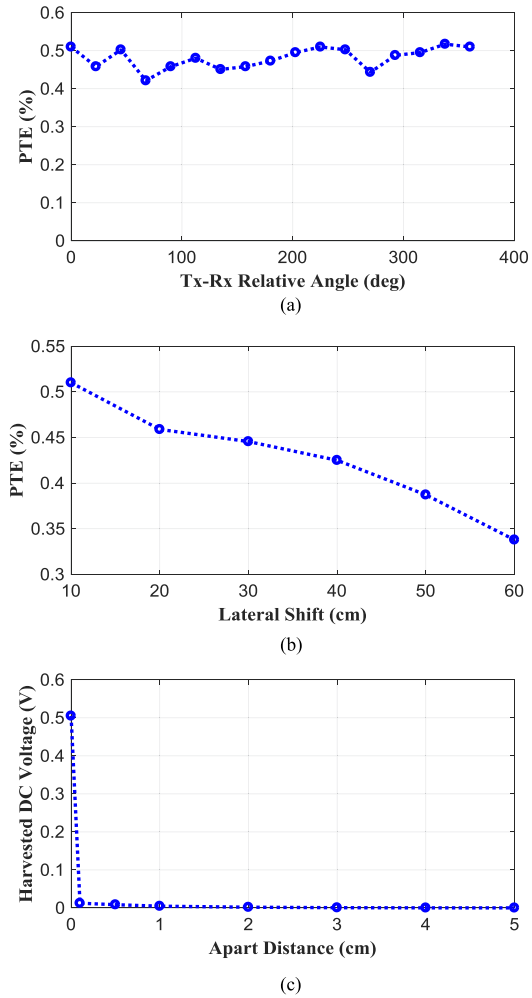


Fig. 21. (a) PTE versus Tx–Rx relative angle. (b) PTE versus Tx–Rx lateral shift. (c) Harvested DC voltage versus apart distance.

## V. CONCLUSION

A new power transfer technique is proposed to replace the conventional inductive/capacitive WPT in transcutaneous power-delivery applications. The proposed technique utilizes the body tissue as the power transmission medium to improve the PTE without violating the IEEE SAR standard, especially when targeting at a miniaturized implanted device deeply inside the body. The measurement result shows that a PTE of 0.39% can be achieved for a 0.3 mm $\times$ 1.3 mm implant locating at a 5-cm insertion depth inside the pork tissue. Compared with the reported 5-cm-range power transfer systems, the proposed technique achieves a PTE of $>2$ times higher even though the implant is much smaller.

The drawback of the proposed method is that the implants should be in contact with the tissue, limiting the application scope. In addition, encapsulation of the implant could be a difficulty, which will be studied in our future work.

## REFERENCES

[1] K. M. Silay, C. Dehollain, and M. Declercq, "Inductive power link for a wireless cortical implant with two-body packaging," *IEEE Sens. J.*, vol. 11, no. 11, pp. 2825–2833, Nov. 2011.

[2] R. F. Xue, K. W. Cheng, and M. Je, "High-efficiency wireless power transfer for biomedical implants by optimal resonant load transformation," *IEEE Trans. Circuits Syst. I, Reg. Papers*, vol. 60, no. 4, pp. 867–874, Apr. 2013.

[3] B. H. Waters, B. J. Mahoney, V. Ranganathan, and J. R. Smith, "Power delivery and leakage field control using an adaptive phased array wireless power system," *IEEE Trans. Power Electron.*, vol. 30, no. 11, pp. 6298–6309, Nov. 2015.

[4] S. C. Tang, T. L. T. Lun, Z. Guo, K. W. Kwok, and N. J. McDannold, "Intermediate range wireless power transfer with segmented coil transmitters for implantable heart pumps," *IEEE Trans. Power Electron.*, vol. 32, no. 5, pp. 3844–3857, May 2017.

[5] R. Jegadeesan, K. Agarwal, Y. X. Guo, S. C. Yen, and N. V. Thakor, "Wireless power delivery to flexible subcutaneous implants using capacitive coupling," *IEEE Trans. Microw. Theory Techn.*, vol. 65, no. 1, pp. 280–292, Jan. 2017.

[6] Y. G. Su, W. Zhou, A. P. Hu, C. S. Tang, S. Y. Xie, and Y. Sun, "Full-duplex communication on the shared channel of a capacitively coupled power transfer system," *IEEE Trans. Power Electron.*, vol. 32, no. 4, pp. 3229–3239, Apr. 2017.

[7] C. K. Chang and C. L. Yang, "Power transfer efficiency improved by thicker coil structure for implanted biomedical IC," in *Proc. IEEE Int. Workshop Electromagn.: Appl. Student Innovation Competition*, May 2016, pp. 1–3.

[8] C. Kim *et al.*, "A fully integrated 144 MHz wireless-power-receiver-on-chip with an adaptive buck-boost regulating rectifier and low-loss h-tree signal distribution," in *Proc. IEEE Symp. VLSI Circuits*, Jun. 2016, pp. 1–2.

[9] F. Jolani, Y. q. Yu, and Z. Chen, "A planar magnetically-coupled resonant wireless power transfer using array of resonators for efficiency enhancement," in *Proc. IEEE MTT-S Int. Microw. Symp.*, May 2015, pp. 1–4.
[10] U. M. Jow and M. Ghovanloo, "Geometrical design of a scalable overlapping planar spiral coil array to generate a homogeneous magnetic field," *IEEE Trans. Magn.*, vol. 49, no. 6, pp. 2933–2945, Jun. 2013.
[11] B. Zhao, N. C. Kuo, and A. M. Niknejad, "A gain boosting array technique for weakly-coupled wireless power transfer," *IEEE Trans. Power Electron.*, vol. 32, no. 9, pp. 7130–7139, Sep. 2017.
[12] A. Ibrahim and M. Kiani, "A figure-of-merit for design and optimization of inductive power transmission links for millimeter-sized biomedical implants," *IEEE Trans. Biomed. Circuits Syst.*, vol. 10, no. 6, pp. 1100–1111, Dec. 2017.
[13] D. Pivonka, A. Yakovlev, A. S. Y. Poon, and T. Meng, "A mm-sized wirelessly powered and remotely controlled locomotive implant," *IEEE Trans. Biomed. Circuits Syst.*, vol. 6, no. 6, pp. 523–532, Dec. 2012.
[14] D. Ahn and M. Ghovanloo, "Optimal design of wireless power transmission links for millimeter-sized biomedical implants," *IEEE Trans. Biomed. Circuits Syst.*, vol. 10, no. 1, pp. 125–137, Feb. 2016.
[15] E. Moradi, T. Bjrninen, L. Sydnheimo, L. Ukkonen, and J. M. Rabaey, "Analysis of wireless powering of mm-size neural recording tags in RFID-inspired wireless brain-machine interface systems," in *Proc. IEEE Int. Conf. RFID*, Apr. 2013, pp. 8–15.
[16] R. Wu, S. Raju, M. Chan, J. K. O. Sin, and C. P. Yue, "Silicon-embedded receiving coil for high-efficiency wireless power transfer to implantable biomedical ICs," *IEEE Electron Device Lett.*, vol. 34, no. 1, pp. 9–11, Jan. 2013.
[17] S. C. Tang and N. J. Mcdannold, "Power loss analysis and comparison of segmented and unsegmented energy coupling coils for wireless energy transfer," *IEEE J. Emerg. Sel. Topics Power Electron.*, vol. 3, no. 1, pp. 215–225, Mar. 2015.
[18] R. Jegadeesan, Y. X. Guo, and M. Je, "Electric near-field coupling for wireless power transfer in biomedical applications," in *Proc. IEEE MTT-S Int. Microw. Workshop Ser. RF Wireless Technol. Biomed. Healthcare Appl.*, Dec. 2013, pp. 1–3.
[19] A. I. Al-Kalbani, M. R. Yuce, and J. M. Redout, "A biosafety comparison between capacitive and inductive coupling in biomedical implants," *IEEE Antennas Wireless Propag. Lett.*, vol. 13, pp. 1168–1171, 2014.
[20] A. Denisov and E. Yeatman, "Ultrasonic vs. inductive power delivery for miniature biomedical implants," in *Proc. Int. Conf. Body Sens. Netw.*, Jun. 2010, pp. 84–89.
[21] S. Ozeri and D. Shmilovitz, "Ultrasonic transcutaneous energy transfer for powering implanted devices," *Ultrasonics*, vol. 50, no. 6, pp. 556–566, 2010.
[22] D. Shmilovitz, S. Ozeri, C. C. Wang, and B. Spivak, "Noninvasive control of the power transferred to an implanted device by an ultrasonic transcutaneous energy transfer link," *IEEE Trans. Biomed. Eng.*, vol. 61, no. 4, pp. 995–1004, Apr. 2014.
[23] S. H. Song, A. Kim, and B. Ziai, "Omnidirectional ultrasonic powering for millimeter-scale implantable devices," *IEEE Trans. Biomed. Eng.*, vol. 62, no. 11, pp. 2717–2723, Nov. 2015.
[24] M. Meng and M. Kiani, "Design and optimization of ultrasonic wireless power transmission links for millimeter-sized biomedical implants," *IEEE Trans. Biomed. Circuits Syst.*, vol. 11, no. 1, pp. 98–107, Feb. 2017.
[25] S. Gabriel, R. Lau, and C. Gabrie, "The dielectric properties of biological tissues: III. Parametric models for the dielectric spectrum of tissues," *Phys. Med. Biol.*, vol. 41, pp. 2271–2293, 1996.
[26] T. H. Lee, *The Design of CMOS Radio-Frequency Integrated Circuits*, 2nd ed. Cambridge UK: Cambridge Univ. Press, 2004, sec. 3.5.1.
[27] P. Vaillancourt, A. Djemouai, J. F. Harvey, and M. Sawan, "EM radiation behavior upon biological tissues in a radio-frequency power transfer link for a cortical visual implant," in *Proc. 19th Annu. Int. Conf. IEEE Eng. Med. Biol. Soc.*, Oct. 1997, vol. 6, pp. 2499–2502.
[28] SMS7630, Shottky Diode, SKYWORKS Company. 2015. [Online]. Available: http://www.skyworksinc.com/Product/512/SMS7630-061
[29] *IEEE Standard for Safety Levels with Respect to Human Exposure to Radio Frequency Electromagnetic Fields, 3 kHz to 300 GHz*, IEEE Standard C95.1-2005.
[30] C. W. Yang and C. L. Yang, "Analysis of inductive coupling coils for extending distances of efficient wireless power transmission," in *Proc. IEEE MTT-S Int. Microw. Workshop Ser. RF Wireless Technol. Biomed. Healthcare Appl.*, Dec. 2013, pp. 1–3.
[31] J. Charthad, M. J. Weber, T. C. Chang, and A. Arbabian, "A mm-sized implantable medical device (IMD) with ultrasonic power transfer and a hybrid bi-directional data link," *IEEE J. Solid-State Circuits*, vol. 50, no. 8, pp. 1741–1753, Aug. 2015.
[32] D. Seo, J. M. Carmena, J. M. Rabaey, M. M. Maharbiz, and E. Alon, "Model validation of untethered, ultrasonic neural dust motes for cortical recording," *J. Neurosci. Methods*, vol. 244, pp. 114–122, 2015.

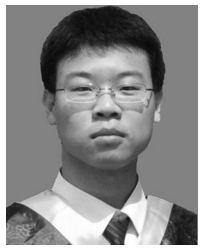

**Pengpeng Chen** received the B.S. and Ph.D. degrees in electronic engineering from Tsinghua University, Beijing, China, in 2009 and 2017, respectively.

He is currently an Engineer with the Beijing Institute of Radio Measurement, Beijing, China. His research interests include radio frequency (RF) transceiver design, including low-power circuit design for wireless body area network applications and ultrawideband RF circuits for radar applications.

**Huazhong Yang** (M'97–SM'99) received the B.S. degree in microelectronics in 1989, and the M.S. and Ph.D. degrees in electronic engineering in 1993 and 1998, respectively, all from Tsinghua University, Beijing, China.

In 1993, he joined the Department of Electronic Engineering, Tsinghua University, where he has been a Full Professor since 1998. He was awarded the Distinguished Young Researcher by the National Natural Science Foundation of China (NSFC) in 2000 and a Cheung Kong Scholar by Ministry of Education of China in 2012. He has been in charge of several projects, including projects sponsored by the national science and technology major project, 863 program, NSFC, ninth five-year national program, and several international research projects. He has authored and coauthored more than 400 technical papers, seven books, and more than 80 granted Chinese patents. His current research interests include wireless sensor networks, data converters, energy-harvesting circuits, parallel circuit simulation algorithms, and nonvolatile computing.

**Rong Luo** received the double B.S. degree in engineering physics and electronic engineering, and the Ph.D. degree in electronic engineering from Tsinghua University, Beijing, China, in 1992 and 1997, respectively.

She is currently an Associate Professor at the Office of Scientific R&D, Tsinghua University. Her research interests mainly include digital system design technology.

**Bo Zhao** (S'06–M'12–SM'17) received the Ph.D. degree in Electronic Engineering from Tsinghua University, Beijing, China, in 2011.

He was a Research Fellow with the National University of Singapore during the years 2013–2015. From 2015 to 2018, he has been an Assistant Project Scientist at the Berkeley Wireless Research Center (BWRC), Department of Electrical Engineering and Computer Sciences, University of California, Berkeley, CA, USA. Since 2018, he has been a Professor with the College of Information Science & Electronic Engineering, Zhejiang University, Hangzhou, China. He has authored or coauthored more than 40 papers and book chapters, including the top-level conferences/journals such as ISSCC, TCAS-I, TPEL, TBioCAS, et al. He holds 15 China patents. His current research interests include miniature radios, wireless power transfer, wearable/implantable radios, and CMOS RF/mixed-signal circuits.

Dr. Zhao is a Technical Committee member of the IEEE Biomedical and Life Science Circuits and Systems Society. He was as the Publication Chair of the 2016 IEEE Biomedical Circuits and Systems Conference. He serves as the TPC of A-SSCC, ISCAS, BioCAS, et al. He was a recipient of the 2017 IEEE TRANSACTIONS ON CIRCUITS AND SYSTEMS Darlington Best Paper Award, the Design Contest Award of the 2013 IEEE International Symposium on Low Power Electronics and Design, the 1000 Young Talents Plan of China, et al.